Numerical Calculation of the Fluid Dynamics of Drop-on-Demand Jets

A numerical method that makes use of the complete incompressible flow equations with a free surface is discussed and used to study an impulsively driven laminar jet. Flow behavior dependence upon fluid properties (characterized by a Reynolds number over Weber number nondimensionalization) is compared for drop integrity purposes. Several variations of square wave pressure history applied at a nozzle inlet are discussed in relation to drop velocities produced and structure of ejected drops. Timewise development of flow both interior and exterior to the nozzle is illustrated through computed contour sequences.

Introduction

Numerical treatment of the fluid dynamics of ink jets is a very ambitious undertaking. A complete description of the flow requires the use of the full Navier-Stokes equations with all associated surface stress conditions. Nonlinearity is present in any finite deformation of a liquid-gas interface and hence a linear analysis can provide only a bare hint of the outcome of a capillary instability. Closed-form solution is out of the question with our present knowledge of the mathematics, leaving us with choices that involve considerable work and are clearly insurmountable without the benefit of fast computation. The strategies one may employ computationally are perhaps many and varied but one can reasonably assume that none is free of extensive and laborious programming and free of potential failure. The need to treat large deformations and break-up into droplets eliminates less general candidate methods. One of the attributes of a successful method is that the required system of equations accurately describes the flow, controlling the motion of the free surface, even to a pinch of the calculation region, followed by smooth continuation of solution with separated regions. This must take place without incurring stiffness problems, numerical instability, or potentially large and scattered truncation errors. Because of the geometric changes, these numerical concerns are particularly stringent. A suitable method must not be limited severely by these factors within the range of flow parameters to be considered.

The basic idea employed here has its origin in some of the earliest large-scale calculations carried out at Los Alamos

Scientific Laboratory when such calculations first became feasible [1]. An Eulerian (fixed) grid system is used to define a discrete form of calculation within the flow region, with the liquid-gas interface defined by a Lagrangian net of points that move with the fluid. This has certain limitations for three-dimensional flow but for a large class of problems, most importantly axisymmetric problems, the net is a string of particles that can be handled easily in the Lagrangian sense. A surface-fitted coordinate system method would perhaps provide a more general treatment with a more direct capacity for extension to three-dimensional flow, but the necessity to redefine the coordinate system with all changes in geometric shape could well make such a scheme intractable when severe distortions occur.

There appears to be little work in the open literature of comprehensive numerical studies of capillary flows. Proposed methods generally fall short of real usefulness in that a single result is given without follow-up calculations to demonstrate program utility. Fortunately, in the work given here, we have had the opportunity to interact with others engaged in active experiments and to be guided by the practical requirements at hand. However, only in recent weeks has it become possible to obtain realistic pressure histories to drive the jets [2]; hence, the results given here do not reflect this new information. We have depended upon estimates of peak pressures and certain constraints inherent in the problem to specify the required pressures. The idealized histories used here surely differ in many respects from actual cases because of acoustic reflections

[®]Copyright 1984 by International Business Machines Corporation. Copying in printed form for private use is permitted without payment of royalty provided that (1) each reproduction is done without alteration and (2) the *Journal* reference and IBM copyright notice are included on the first page. The title and abstract, but no other portions, of this paper may be copied or distributed royalty free without further permission by computer-based and other information-service systems. Permission to *republish* any other portion of this paper must be obtained from the Editor.

J. E. FROMM

within the driving chamber [3] and, for that matter, particular attributes of the piezo driver. Potentially interacting studies could be carried out in the future that could evaluate entire systems, but the economics of such an extensive study is not warranted in terms of current needs. For this reason, it is perhaps appropriate to limit the study to certain idealized cases, chosen to provide guidelines relative to the adjustable parameters of the problem.

We consider first a given geometric configuration with the same pressure histories but with variation of the fluid properties (viscosity, density, and surface tension coefficient). Next, we consider fixed fluid properties with pressure history variations such that higher velocities are achieved. In the latter case, there are a number of aspects of the flow behavior that define its usefulness for drop-on-demand ink jet printing. These principally include the absence or presence of shadow drops and an adequate drop velocity. To simultaneously achieve a sufficiently high velocity and drop integrity is the realm of experiment, since many variations of driving voltage and hence pressure can be tested rapidly. Computationally, this would be impossible because the window of desired behavior is probably too narrow to be isolated by this approach alone and may not be achievable in the cylindrical nozzle case at all with simply structured pressure histories.

In the calculations, we assume that the pressure histories vary in time but are uniform across the inlet section of the nozzle. Currently, there is no way to know if this is true. Since the inlet section diameter is very small compared to the chamber diameter, it is assumed that the pressure can vary little across the face of the inlet. There is, however, no guarantee that this is the case. A calculation of the dynamics within the chamber, while of interest in itself, could probably not have sufficient resolution to modify the assumption of uniformity of pressure at the inlet. Numerically, one could, with the methods described here, readily test other assumptions, but we have found no reason to do so.

In regard to the boundary layer in the nozzle, we assume on inflow that the boundary layer grows from the inlet. This implies that the vorticity is zero over the inlet cross section. If, on the other hand, fluid is drawn backward into the chamber, a "slow change" condition is assumed. Basically, this requires that no radial velocities exist at the chambernozzle juncture, but the boundary layer can move into the chamber.

We do not attempt to deal with wetting contact angles in any rigorous manner. There are two conditions of interest here where ad hoc treatment must be justified. One is that wetting of the exterior of the nozzle outlet is not permitted in the computation. This would seem to be important at early phases of drop ejection, but this is the very time that driving pressures are highest, and hence it is reasonable to assume that the presence of a contact circle exterior to the outlet would have little influence upon the drop dynamics. While the magnitude of the contact pressure could be large, it acts upon a very localized region compared to the driving pressures from the chamber. For a very weak driving pulse, one would expect some effect on drop behavior from a wetting exterior contact, but not for the high ejection velocities of interest here.

The second condition that must be dealt with is that of a moving contact line that arises when fluid is drawn into the chamber by a pressure differential with ambient external pressure. The problem here is not one of influencing drop integrity or dynamics, since by this stage the incipient drop is well on its way forward and is quickly becoming isolated from any flow that is going on within the nozzle. The problem is more one of continuation of the numerics in an empirical manner, at least to the point of detachment. Here, we have considered simply requiring the contact circle to remain at the outlet. This is the simplest ad hoc condition one can impose, but unfortunately in some cases the suction may be large, so that only a thin unresolvable layer of fluid clings to the nozzle interior. For this reason, we have found it necessary to allow the contact line to move, only to the extent that calculation can proceed. This works in a satisfactory manner up to detachment, but the final behavior of the remaining meniscus becomes somewhat artificial since a 90° contact angle emerges as a final state with only a partially filled nozzle. In the real case, wetting would return the fluid to the outlet. The complex interplay of forces that one would have to take into account to give a complete treatment of the meniscus is not justified here since our interest is primarily the behavior of the detached drop.

There are a number of other unanticipated problems that arise in numerical computation. For example, if the driving pressure is pushed too high, wavelets appear on the jet surface that require higher resolution than one wishes to impose for a reasonable length calculation. Also, the peak driving pressure for a given drop velocity is a strong function of the nozzle length. It is a function of the volume of fluid in the nozzle, which must be set into motion, and also the added viscous drag of a longer nozzle. To limit the computational region and hence computation time, a short nozzle is preferred. Indeed, the "equivalent" cylindrical length for nozzles used in practice is short. This, however, leads to problems when a retraction occurs that opens backward into the chamber or beyond the calculation range. Here again, an ad hoc treatment is called for, or else a section of the chamber must be included in the calculation domain. Unfortunately, the latter brings in a number of new problems. A nozzle length equal to the jet diameter seems to be a good compromise, allowing for a reasonable retraction length and yet not requiring unrealistic

pressures relative to DOD experiments. With this choice, we avoid retraction into the chamber region.

One other consideration in regard to a discrete calculation is that of separation of the flow when the drop breaks away from the jet column. This must occur at one radial mesh distance at the least; otherwise there are not enough computational data to continue. With 20 mesh points for a nozzle radius, break-off occurs numerically at five percent of the jet diameter. Numerical experiments show that this is satisfactory because the remainder of the excursion to zero radius occurs very soon after this point; the high azimuthal curvature of the surface causes ever larger pressures and faster convergence. Clearly, if we were willing to invest more time in calculation, we could look very closely at break-up, but again it is not an important issue for the accuracy here required.

Governing equations and general aspects of the numerical method

Unlike the numerical methods developed in Ref. [1], we here wished to make use of a streamfunction. The reason for this is that flow through a nozzle can become very awkward without a streamline defining the solid bounding surface. The programs were initially tested with periodic boundary conditions [4], and a preliminary drop-on-demand form of calculation was given in Ref. [5]. The numerical method used here is as given in these references but will be reviewed. Of possible interest to the reader are some new developments in the numerical programs in connection with other applications [6, 7]. The newer methods were not employed here because there seemed to be no need to do so. Deficiencies in the older method were not of a fundamental nature but related to numerical algorithms and redundant computation that was inefficient. With minor updates in the algorithms, the older programs were revived for this work.

The pertinent equations for calculation in the interior are the Navier-Stokes equations for radial (r) velocity v and axial (z) velocity u. These are

$$\frac{\partial v}{\partial t} + \frac{\partial uv}{\partial z} + \frac{1}{r} \frac{\partial v^2 r}{\partial r} = -\frac{\partial \frac{P}{\rho}}{\partial r} + \nu \left[\frac{\partial^2 v}{\partial z^2} + \frac{\partial}{\partial r} \left(\frac{1}{r} \frac{\partial vr}{\partial r} \right) \right],$$

$$\frac{\partial u}{\partial t} + \frac{\partial u^2}{\partial z} + \frac{1}{r} \frac{\partial u v r}{\partial r} = -\frac{\partial \frac{P}{\rho}}{\partial z} + \nu \left[\frac{\partial^2 u}{\partial z^2} + \frac{1}{r} \frac{\partial}{\partial r} \left(r \frac{\partial u}{\partial r} \right) \right], \tag{1}$$

where P is the pressure, ρ the density, and ν the kinematic viscosity. In this axisymmetrical form of the equations, the vorticity is

$$\omega = \frac{\partial v}{\partial z} - \frac{\partial u}{\partial r},\tag{2}$$

and hence

$$\frac{\partial \omega}{\partial t} + \frac{\partial u\omega}{\partial z} + \frac{\partial v\omega}{\partial r} = \nu \left[\frac{\partial^2 \omega}{\partial z^2} + \frac{\partial}{\partial r} \left(\frac{1}{r} \frac{\partial \omega r}{\partial r} \right) \right]. \tag{3}$$

In Eq. (3), it was necessary to make use of the incompressibility condition

$$\frac{\partial u}{\partial r} + \frac{1}{r} \frac{\partial vr}{\partial r} = 0. \tag{4}$$

If we define the streamfunction by the set

$$vr = -\frac{\partial Q}{\partial z}$$
 and $ur = \frac{\partial Q}{\partial r}$, (5)

we are led through (4) to the streamfunction equation

$$\frac{\partial^2 Q}{\partial z^2} + r \frac{\partial}{\partial r} \left(\frac{1}{r} \frac{\partial Q}{\partial r} \right) = -r\omega. \tag{6}$$

Also, Eqs. (1) inserted into (4) leads to

$$\frac{\partial^2 P}{\partial z^2} + \frac{1}{r} \frac{\partial}{\partial r} \left(r \frac{\partial P}{\partial r} \right) = -G,\tag{7}$$

where

$$G = \frac{\partial^2 u^2}{\partial r^2} + \frac{2}{r} \frac{\partial u v r}{\partial r} + \frac{1}{r} \frac{\partial^2 v^2 r}{\partial r^2}.$$
 (8)

This system of equations is more than is needed for solution of many initial-boundary value problems, but by considering the whole system, we have greater flexibility in meeting requirements of a complex time-varying boundary. Our problem here is to consider the time evolution of flow that begins at rest in a cylindrical nozzle geometry. The initial boundaries are the containing cylindrical surface, a disk-shaped surface which is the interface with a large chamber of the same fluid and another disk-shaped surface that is the interface with a gas. The latter interface is allowed to move under certain constraints dealing with the properties of such a surface. Taking symmetry into account, we may use the center line of the cylinder as a boundary. The best representation of the flow in the interior is in terms of streamlines such that the center line is a reference (zero) streamline and the cylindrical surface takes on a streamfunction value appropriate to the flow rate. The flow rate is in turn determined by the applied pressure at the chamber-nozzle interface and also the inertial and viscous properties of the fluid itself. To obtain the appropriate streamfunction value at the cylindrical wall, we integrate the second of Eqs. (1) over a control volume making use of the second of Eqs. (5). This may be the entire fluid volume of interest or some subsection of the volume so long as we know precisely the required quantities on the boundaries of the domain we choose. Upon integration, we obtain

$$\left(\frac{dQ}{dt}\right)_{r_0} = \frac{1}{z_0} \int_0^{r_0} r(u_L^2 - u_R^2 + P_L - P_R) dr - \frac{\nu r_0}{z_0} \int_0^{z_0} \omega_{r_0} dz.$$
(9)

Because of the conservative form of the momentum equation, the volume integral becomes a surface integral. It states that the time rate of change of streamfunction at the cylindrical wall (r_0) depends upon the pressure gradient and kinetic energy gradient over the length (z_0) , summed over disk-shaped areas at the left (L) and right (R) of our chosen control volume. In addition it depends upon the viscous drag at the no-slip cylindrical surface expressed as a sum of the vorticity present at that surface. Thus, we have the means to begin calculation, noting that O will forever be zero at the axis, as is the vorticity. At the inlet, the vorticity is also set to zero except at the cylindrical surface, while the inflow velocity is taken to be uniform. This uniform flow velocity follows from the gross application of the second of Eqs. (5) and then intervening Q values follow from this velocity. The same applies at the outlet at the initial instant.

Our control volume can initially be the entire volume of fluid in the nozzle since a known ambient pressure condition exists at the outlet. Unfortunately, things become more complicated after the free surface begins to deform.

In Figure 1 we portray a late stage of solution to which we aspire. We note that a meniscus can exist, along with a flow region that is completely enclosed by a free surface and separated from the fluid in the nozzle. Note in Fig. 1 that we give a symbolic representation of the global system of variables and their layout on a discrete grid as they are defined for interior flow. Our control volume as employed in Eq. (9) refers to this global system and hence must be chosen to lie inside the meniscus at all stages of calculations. This is preferred to using a deformed surface as a control volume boundary. We, of course, will have access to all variables at all times throughout the calculation and specifically at some constant z distance in the nozzle for a boundary of our control domain.

We now know how to get the streamfunction values at the solid cylindrical surface and at the inlet, but what about streamfunction values on the free surface once it deforms away from a global grid line? These surface values of Q are required for solution of the elliptic Eq. (6). Here the procedure is to obtain tentative u and v values by small forward steps in time applied to the momentum equations. Then, integrating along any convenient grid lines using Eqs. (5), we may obtain Q at grid extensions to the free surface. By this means, we have our required boundary condition for Eq. (6) and can also define a normal velocity at the surface.

We have found it convenient to introduce a finer net of points at the surface by means of which information is exchanged with the interior. Thus, the Q values are spread among local surface points by interpolation. To each of the surface points, we may assign other variable values. Further, allowing these points to be origins of local coordinate systems

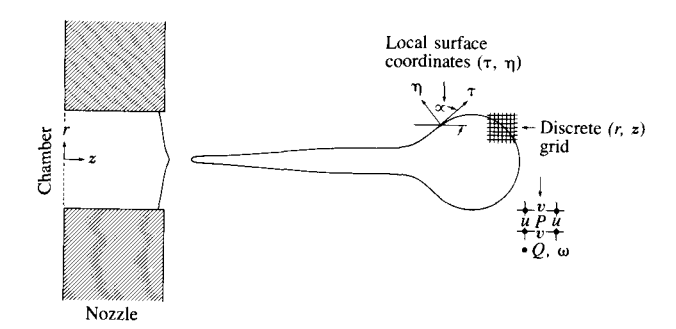


Figure 1 Nozzle geometry and a typical jet configuration with symbolic representation of the computational grid.

oriented relative to an outward normal at the surface, we can readily define surface boundary conditions. Knowing the angular orientation (α) of these local coordinate systems, with the global system, permits transfer of information between systems by rotational transformations. With reference to Fig. 1, then, we can now write the required surface conditions in the (τ, η) frames as indicated. The normal stress or pressure jump condition at the surface relative to an ambient gas pressure $(P/\rho)_0$ is given by

$$\frac{P}{\rho} - \left(\frac{P}{\rho}\right)_{0} = \frac{\sigma}{\rho} \left(\frac{\cos \alpha}{r} - \frac{\partial \alpha}{\partial \tau}\right) + 2\nu \left(\frac{\partial u_{\eta}}{\partial \eta} + u_{\tau} \frac{\partial \alpha}{\partial \eta}\right), \tag{10}$$

where σ is the surface tension coefficient. Now $\partial \alpha/\partial \tau$ is the familiar surface curvature or variation of the angle of the tangent to the surface as we move along the surface; $\cos \alpha/r$ is the curvature about the axis of symmetry. The terms on the far right of Eq. (1) are viscous damping terms that produce second-order effects in the flows considered here. We here include only the first of these terms as is often the case in works found in the literature.

Clearly, with α known for each surface net point, the effects of curvature upon the pressure differential at the surface may be calculated. It is convenient to take the ambient pressure as zero and then these quantities give the pressure directly. A tactic to use to compute the normal derivative of u_n is to first select a near-surface mesh point and find the surface net point that is closest to that interior point. Using the appropriate α , one then carries out a rotational transformation to obtain u_n in the interior. Knowing the surface u_n obtained from Q (i.e., $u_{\eta} = -1/r \, \partial Q/\partial \tau$) one may then approximate the gradient. Here, we assume that the closest approach of the surface to the selected interior grid point approximates the surface normal through that grid point. A similar procedure is used to obtain the tangential velocity at the surface from surface Q values $(u_{\tau} = 1/r \partial Q/\partial \eta)$ and those calculated at the interior through the elliptic Eq. (6).

The vorticity values on the right of (6) are obtained by forward marching Eq. (3) as is done with the momentum

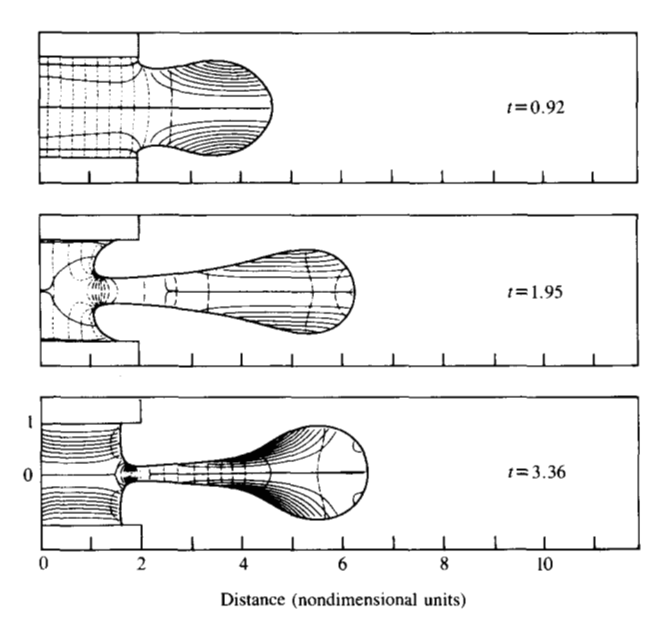


Figure 2 Time sequence of jet development for R/W = 2 with pressure histories as in Table 1 and plot data as in Table 2.

equations. The origin of most of the vorticity is "generation" in the boundary layer along the cylindrical surface of the nozzle. To a secondary extent, vorticity is also derived from the free surface. It follows from the definition of vorticity and the tangential stress condition that

$$\omega = 2 \left(\frac{\partial u_{\eta}}{\partial \tau} + u_{\tau} \frac{\partial \alpha}{\partial \tau} \right). \tag{11}$$

This free surface vorticity is included in the calculations but its function there is somewhat mysterious and still under study.

Finally, it will be noted that the pressure is required in the fluid in order to allow inclusion of pressure gradients in the tentative forward march values of the velocities. This is a painful part of the calculation since it is complicated and is in the final analysis required only to get the streamfunction boundary condition. The reward is that it is nice to know what the internal pressures are. We not only have a difficult-to-calculate right-hand side to the pressure Poisson's Eq. (7), but the normal derivative conditions at the no-slip surface of the nozzle must be taken into account. That is,

$$\frac{\partial \left(\frac{P}{\rho}\right)}{\partial r} = \nu \frac{\partial \omega}{\partial z} \tag{12}$$

at $r = r_0$ and at the axis r = 0,

$$\frac{\partial \left(\frac{P}{\rho}\right)}{\partial r} = 0. \tag{13}$$

Table 1 Square wave pressure histories at nozzle inlet for results given in Figures 2, 3, and 4.

R/W = 2		R/W =	= 3	R/W = 4	
Time	P/ρ	Time	P/ρ	Time	P/ρ
0.00-0.12	-30.0	0.00-0.10	-40.0	0.00-0.12	-30.0
0.12-0.68	+50.0	0.10 - 0.71	+40.0	0.12-0.69	+40.0
0.58-1.27	-40.0	0.71 - 1.21	-40.0	0.69 - 1.17	-40.0

At the free surface and at the inlet, the pressure is itself given.

Surface particle motion comes about in calculation by applying the Lagrangian expressions

$$\frac{dz}{dt} = u$$
 and $\frac{dr}{dt} = v$, (14)

where u and v follow from rotational transformations of u_{τ} and u_{η} .

We have given a somewhat cursory description of the numerical procedure. The interested reader should consider the references given, particularly Ref. [6], which gives finite difference expressions and other numerical details.

For studying the results that follow, it should be noted that we do the calculations in nondimensional form with the nozzle radius r_0 as a reference unit length. A reference velocity

$$v_0 = \left(\frac{\sigma}{\rho r}\right)^{1/2} \tag{15}$$

and an associated reference time scale

$$t_0 = \left(\frac{\rho r^3}{\sigma}\right)^{1/2} \tag{16}$$

lead to a single parameter that contains all the fluid properties. That is, with R the Reynolds number and W the Weber number, we have

$$\frac{R}{W} = \left(\frac{\sigma r}{\rho \nu^2}\right)^{1/2}.\tag{17}$$

To make the differential equations dimensionless, it is only necessary to replace ν by W/R and σ/ρ by unity. A final note is that we often refer to P/ρ simply as the pressure in discussing the results.

Discussion of results

Unlike in the laboratory, we here look at only a single drop formation. In real time, the elapsed period encompassed by the numerical calculation may be on the order of 100 microseconds. By contrast, indicating some measure of the com-

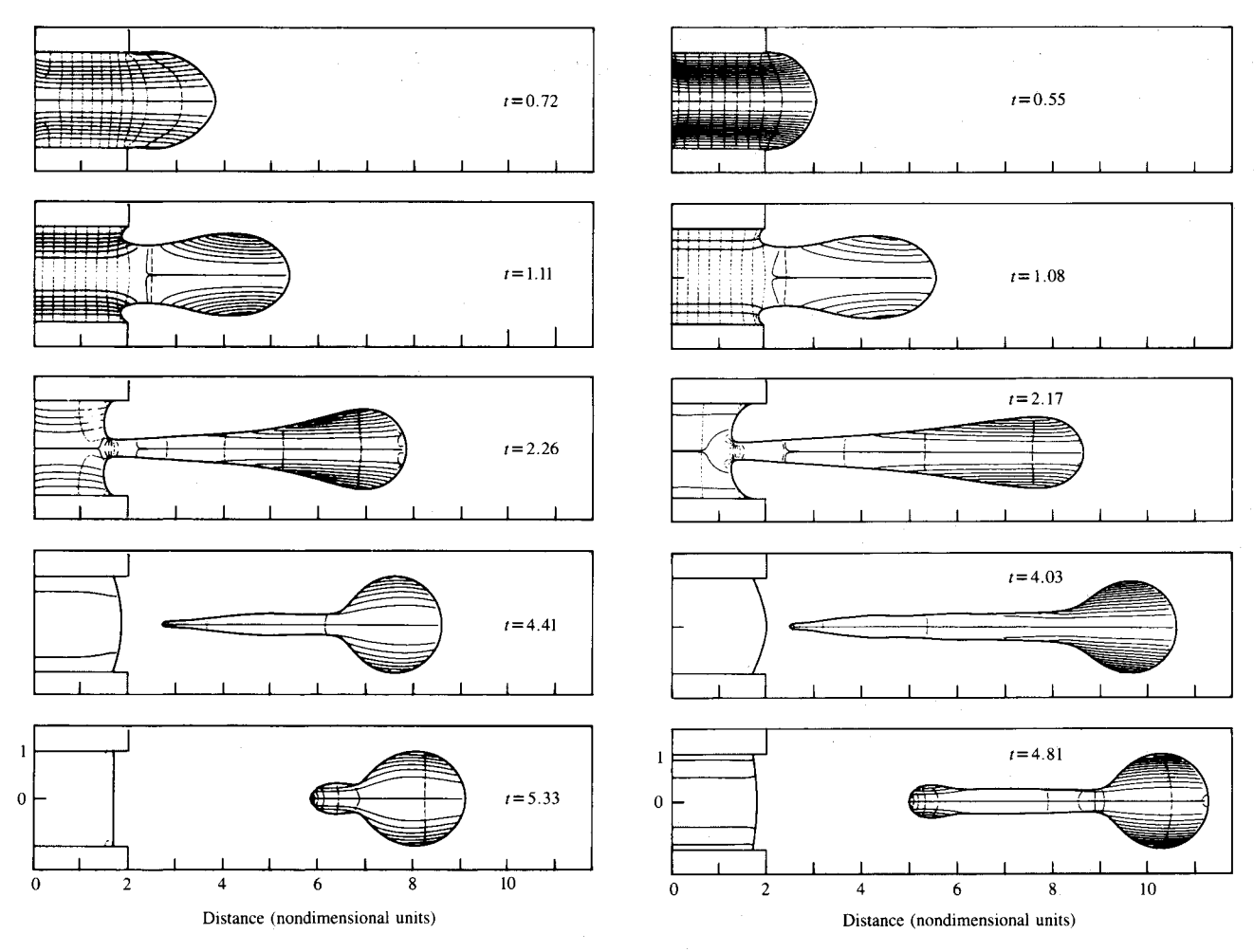


Figure 3 Time sequence of jet development for R/W = 3 with pressure histories as in Table 1 and plot data as in Table 3.

Figure 4 Time sequence of jet development for R/W = 4 with pressure histories as in Table 1 and plot data as in Table 4.

plexity of the fluid dynamics involved, the calculation time is on the order of two hours. The simplicity of appearance of an evolving laminar jet is deceptive, giving no indication of the underlying mathematical theory associated with a description of the dynamics. With the aid of computer graphics, we can display both the external appearance of the drop formation and simultaneously the invisible forces and velocities responsible for what we observe. A further deception lies in that once a numerical result is at hand, the reaction is "why of course" it is what one would have expected. This is in fact the basic intent of the study, to provide us with the confidence that we really understand what is going on and, in addition, to fill in gaps in our understanding that we perhaps did not realize existed.

The sequences of solutions given here are direct output of the computer graphics. Selection of the times illustrated is intended to give contrasting states of the flow, yet provide some degree of continuity of successive times. In all cases, streamlines and isobars are presented in the plots and an associated table of plot increments is given in the text. Since the velocity and pressure magnitudes vary considerably, plot intervals will also vary considerably. It is therefore important that the reader make full use of the tables when studying the plots. Otherwise, some false impressions may arise.

Streamlines are the solid lines of the plots and isobars of pressure are the dashed lines. Reverse flow into the chamber is distinguished by tick marks on the solid streamlines, while in the isobars the pressures below ambient are short dashes relative to the longer dashes that define pressures above and at ambient pressure. Unfortunately, the tick marks for negative valued streamlines do not show up well in the reductions of the figures. Generally, here, they simply give a darker hue to the line. A close examination of the tables of increments and extremum values can be used to overcome this deficiency. Further, the reverse flow associated with negative valued streamlines will be recognizable from discussions that follow.

Table 2 Plot parameters for Figure 2.

Time	Plot interval Q	Q_{min}	Q_{max}	Plot interval P	P_{min}	P_{max}
0.92	1/8	-0.18	1.26	4	-40.00	3.12
1.95	1/32	-0.04	0.22	1/2	-2.58	3.18
3.36	1/128	-0.00	0.08	1/2	-0.83	5.90

The first group of flow sequences are intended to show variations to be expected with change in fluid properties. In terms of the scaling of the problem here adopted, these are given in the order of R/W = 2, 3, 4 in Figures 2, 3, and 4. The contrast in the flows with this selection of R/W values is very dramatic and we were obliged to deviate slightly from our original plan to have an identical set of pressure histories. In Table 1, we tabulate the pressures and times associated with the square wave histories applied at the nozzle inlet. In the numerical program, the input parameters are the sequence of pressure magnitudes but these are timed by certain characteristics of the flow. Here, we have allowed a small initial retraction, with below-ambient pressure at the inlet until a 0.1 unit retraction of surface from the outlet has been achieved. At this point, the follow-up positive pressure is applied until the flow volume from the nozzle is equivalent to a spherical drop of unit radius. At this point, the pressure at the inlet is again reversed and held at the negative value until the overall applied impulse

$$\int_{0}^{t} \frac{P}{a} dt = 0. {18}$$

From this point onward, the jet is simply reacting to the applied impulse through the action of inertia and through its own viscosity and capillarity. The time required for the initial small retraction is unaffected by differences in the R/W parameter. This is because the retraction is small and only inertia of the fluid in the nozzle is involved; viscosity does not have sufficient time to act to any significant extent. Less time is required, however, to eject a given volume as the R/W parameter is increased. The reason for using 50 units of driving pressure instead of 40 with R/W=2 was that ejection was considerably weakened by the higher viscosity. The time required to return the net impulse to zero, in all cases, is simply proportional to that impulse that had to be applied to get the desired volume of flow in the first place.

In Fig. 2, for R/W=2, the initial time illustrated is one in which final retraction is already underway. The isobars are spaced at four units of pressure with ambient pressure $(P/\rho=0)$ occurring at the last isobar on the right that passes through a contracted zone of the forming drop. The highest pressure here (refer to **Table 2**) is not in the neck but at the front tip of the drop that is somewhat pointed in shape at this early

time. The capillary forces have not yet caused rounding of a distorted early shape (two units of pressure define a spherical drop of unit radius, one unit for each principal curvature). The flow lines are self-explanatory except that we may note here that retracting flow begins in the boundary layer where flow reversal occurs first, because of fluid inertia. The first streamline inward from the nozzle wall represents flow to the left, the next line inward radially is a dividing streamline, as is the central streamline. This means that the flow inside the nozzle is almost stagnant. One must, however, keep in mind that in the axisymmetric case, the gradient in the streamlines is not a direct measure of the velocity since we must also divide by the radius. Thus, the spread in lines near the axis only partially implies slower flow there. At this earliest time, the flow speed along the axis, at the tip of the jet, is the greatest.

At the second time of Fig. 2, the applied pressures have all been removed and the inlet sits at ambient pressure. Belowambient pressures exist in the nozzle because of the concave curvature in the annular region about the neck of the jet. There is some forward flow in the nozzle because of the pressure gradient associated with the concave annular region. The neck of the jet, at its narrowest point, has the highest pressure. This is just forward of the dense collection of isobars. From there, the pressure drops, moving forward, with the two-unit isobar through the center of the inflating drop. Pressure again rises toward the jet leading edge. Any streamlines which connect to the center line of the jet are separation streamlines, so one may assume that flow, while too small to be indicated, is in a clockwise sense in the contraction zone.

The final time illustrated for R/W=2 shows a condition in which the imparted forward momentum is almost gone. The forward motion of the jet is little changed from the earlier time. The flaring internal motion shows that capillary forces have full command and are simply reducing the overall surface to a minimum. This involves inflating the bulbous region at the expense of the fluid in the contracted zone and reducing the meniscus to a cylindrical disk (physically at the nozzle outlet). The pressure plot interval is the same as at the earlier time and a similar interpretation applies except that the added contraction has led to higher pressures. The concave curvature at the flare holds down the pressure so that the last isobar in

Table 3 Plot parameters for Figure 3.

Time	Plot interval Q	Q_{min}	Q_{max}	Plot interval P	P_{min}	P_{max}
0.72	1/4	0.00	2.12	4	-42.63	2.00
1.11	1/8	-0.87	1.12	4	-40.00	3.15
2.62	1/32	-0.01	0.29	1	-5.89	4.89
4.41	1/32	-0.05	0.24	4	0.00	40.26
5.33	1/32	-0.08	0.23	2	-0.09	21.55

Table 4 Plot parameters for Figure 4.

Time	Plot interval Q	$Q_{\it min}$	Q_{max}	Plot interval P	P_{min}	P_{max}
0.55	1/8	0.00	1.98	4	-0.51	40.0
1.08	1/4	-0.75	1.37	4	-40.0	2.79
2.17	1/16	-0.02	0.52	1	-3.78	4.73
4.03	1/32	-0.03	0.41	4	0.00	40.5
4.81	1/32	-0.07	0.42	1	0.00	10.0

this region is two units, as is that through the central region of the forming drop, thus accounting for the extra isobars formed in the upstream direction. The forming drop is becoming isobarometric. A remnant of forward motion exists at the front of the forming drop. At a later time, the leading edge may move backward in a weak oscillation in the drop shape. The flow within the nozzle is all forward in the last illustration and if wetting were properly taken into account, the contact line would migrate to the outlet. Again, the dense collection of isobars at the contraction is a consequence of passing from a below-ambient pressure in the concave annular region to the highest pressure (on the order of six units) just forward of the collection.

In Fig. 3 (R/W=3), the first time illustrated is for t=0.72. The positive pressure pulse has just been terminated (see Table 1) and the final negative phase of inlet pressure is active. Surprisingly, the lowest pressure in the field of values is less than that applied at the inlet (see **Table 3**). It occurs near the inlet nearly at the cylindrical surface of the nozzle. It is a consequence of vorticity associated with our requirement that the boundary layer begins at the inlet. There is a slight squeeze in the flow related to an incipient flow separation. Note that even though the inlet pressure is negative, forward motion persists because of inertia. The ambient pressure isobar is the most forward one so that positive pressures exist only in a cap-shaped region at the front of the jet.

At the second time illustrated in Fig. 3, the flow in the nozzle is reversed and a reversed boundary layer is developing. With a decay of the original boundary layer, the lowest pressure is now the input pressure of -40.0 units. The remaining

details of this second time illustrated and the following time are similar to those of Fig. 2. Small surface deformities at the front of the jet, at the latter time, are responsible for pressure variations manifested in localized isobars.

At the fourth time illustrated in Fig. 3, break-off has occurred. The meniscus within the nozzle has bulged forward because of inertia and is now in the process of returning to a disk shape through flow toward the chamber. A very high pressure exists at the end of the tail of the forming drop, as is evident in Table 3. Unfortunately, this high pressure results in a large plot increment and hence more detailed isobars are not given in the illustration. Flaring of the streamlines within the drop is, of course, because the tail is rapidly being assimilated by the drop. But, unlike R/W=2, the flaring is only at the trailing part of the drop and directly forward motion persists at the leading part of the drop.

The last time illustrated in Fig. 3 is prior to consolidation of the drop. A remnant of the tail is still present but it is catching up to the main body of the drop, as is evident in the density and curvature of the streamlines. A high pressure and high pressure gradient still exist at the end of the tail. The pressure has diminished by about half that at the earlier time (see Table 3). Unlike the case of R/W = 2, the drop will continue forward motion. Our intent is to come back and review this and other differences after consideration of the R/W = 4 case.

With reference to **Table 4**, the reader should now be able to follow the details of the flow behavior illustrated in Fig. 4. Corresponding to the "dumbbell" final illustration in Fig. 3, a

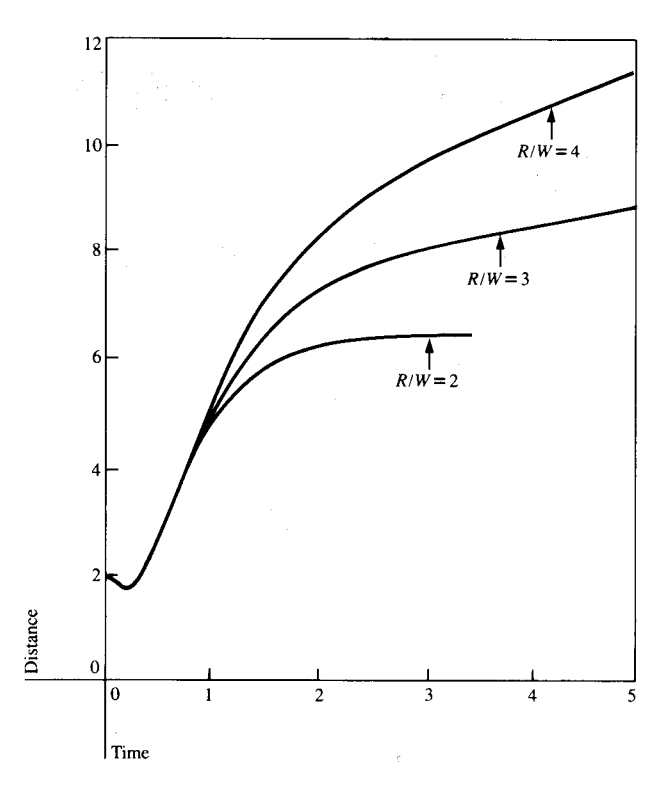


Figure 5 Motion of leading edge for jets illustrated in Figs. 2, 3, and 4.

"baby rattle" configuration emerges, for R/W=4, in which a small drop is linked to the main drop by a cylinder of liquid. There is some contraction just behind the main drop and hence a rise in pressure there. Generally, the small drop catches up to the main drop before a complete pinch-off occurs here. This behavior is observed in experiments.

Reviewing now the calculations for R/W = 2, 3, 4, we may conclude that higher drop velocities are obtained with larger R/W when an equivalent impulse is applied. To give a measure to the differences to be expected, we plot, in Figure 5, a history of the position of the leading edge of the jets. For the pressure histories given in Table 1, we note that for R/W = 2, flow essentially stops; the fluid will collect into a suspended drop (in the absence of gravity here). The velocity histories, again measured at the leading edge of the jet, are given in Figure 6. The noise in the velocity histories is mostly truncation error in the numerical calculation but the larger variations near maximum velocity are perhaps associated with local readjustment at the leading tip because of distortion from a locally spherical shape. Break-off occurs in the R/W = 3 case at t =4.15 and for R/W = 4 at t = 3.95. Plots of the decay of contraction radii will be shown in some cases to be discussed in the following. After break-off, there is a slight increase in the velocities of the leading edge. This is simply the forming drop settling down to some mean velocity after detachment. The higher velocities of the nonuniform distribution are, of course, in the rapidly moving tail. Since we used flow volume

to determine when the applied positive pressure was to be removed, the actual impulse was somewhat larger for the smaller (more viscous) R/W values while the final drop volume was slightly less. Thus, the differences for truly equal impulse would be even somewhat more than illustrated. This, however, is only one sample impulse comparison. With a larger impulse, one would expect R/W = 3 to begin to look like Fig. 4. Some results suggest, however, that the interconnecting cylinder of fluid between small and large drops becomes thinner, i.e., contains less volume of liquid if R/W is smaller. We continue then by considering fixed fluid properties (R/W = 3) with modified applied pressures.

If we simply increase the magnitude of the positive part of the pressure history, we find that we must modify the volume flow cut-off to maintain a corresponding drop volume. Previously, we had chosen the cut-off to be a volume with one nozzle diameter. In the following, we have reduced the cut-off volume to a volume corresponding to a ¾ diameter of the nozzle. Figure 7 shows what happens to the pressure history with change in the volume flow cut-off. The pressure history of the Fig. 3 run is given along with histories for the faster cut-off volume.

Note how the (¾) cases involve shorter and shorter times for the 60-, 80-, and 100-unit peak pressures. The entire period of the pressure cycle is shorter than for the unit volume cutoff of the Fig. 3 run; all terminate at the same time. As it turns out, the run with the 60-unit peak pressure differed little physically from the result of Fig. 3. This is because the lower pressure acted for a longer time. Figure 8 gives the radius of contraction of these two runs. The longer period, before contraction begins, with the unit cut-off case reflects the pressure history. Finally, drop sizes differ somewhat with a larger drop for the unit cut-off case.

We continue by comparing statistics for the 60-, 80-, and 100-unit peak pressure runs and will then include a late time sequence for the latter of these. Surprisingly, the contraction radii curves were essentially identical. While successively larger final drops emerged with increased peak pressure, the associated longer negative pressures (to reduce the impulse to zero) succeeded in bringing about essentially equal break-off times. Normalized volume flow curves are given in Figure 9. These are the flow passing the outlet of the nozzle (in either direction). They reflect the fact that the nozzle does not refill like it would physically. Note that in Fig. 9, we also give a final normalized drop size. This size is based on the assumption that any multiple droplets will ultimately re-merge at some late time. That is, if drops are multiple at some stage in the calculation, their volumes are summed. In Figure 10, we show distances of the leading edge of the jets for the 60-, 80-, and 100-unit peak pressure runs. Figure 11 gives the associated velocity histories.

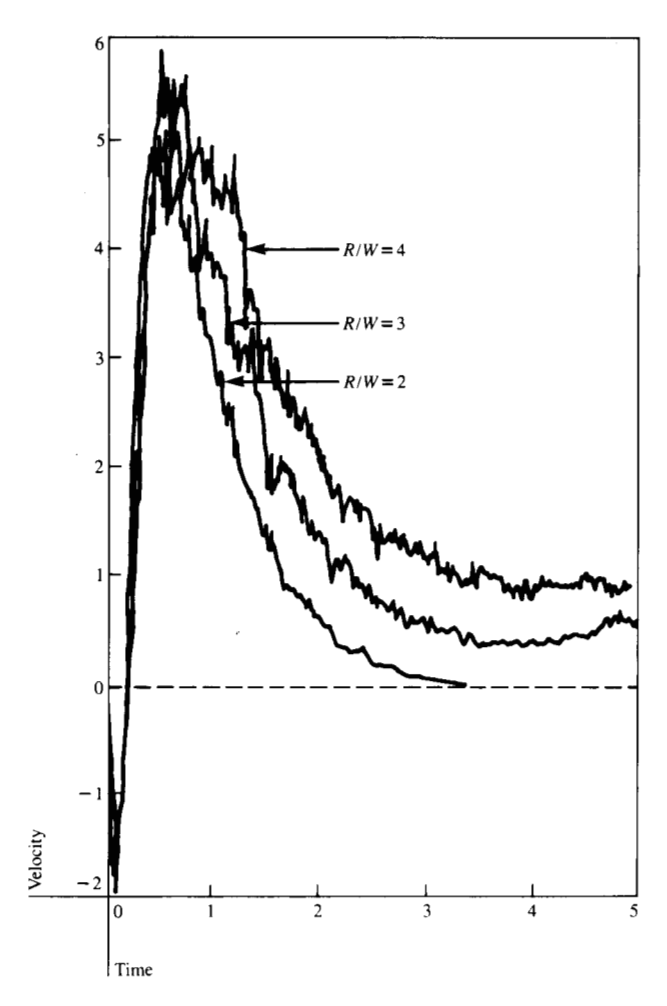


Figure 6 Velocity of leading edge for jets illustrated in Figs. 2, 3, and 4.

In Figure 12, the late time behavior of the 100-unit peak pressure case is given in contour map form. Table 5 gives the associated plot data for the selected times. A transition of behavior exists for this range of peak pressures. For the 60unit case, a single drop developed directly from the tail as in Fig. 3. In the 80-unit case, a satellite drop like that in Fig. 12 emerges but the intermediate ripple is not present. The average satellite velocity was higher than that of the main drop in all cases where they occurred in the present study. Note that the leading edge velocity (Fig. 11) for the 100-unit case increases at late times. This is a consequence of the intermediate ripple merging with the leading segment near the same time that the trailing segment detaches. Thus, the now-combined leading drop is set into oscillation, as is evident from the shape and streamlines present. The satellite drop is also undergoing oscillations that are less obvious at the late times illustrated.

It is perhaps not strange that the final drop velocities of the 60-, 80-, and 100-unit pressure cases are almost the same since

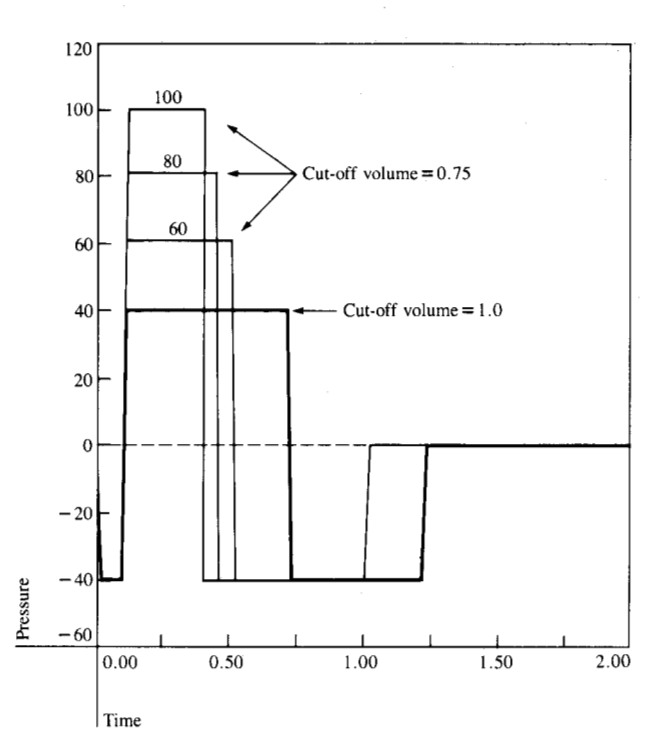


Figure 7 Pressure histories of a series of calculations for R/W = 3. Cut-off volume = 1.0 case is pressure history for jet of Fig. 3.

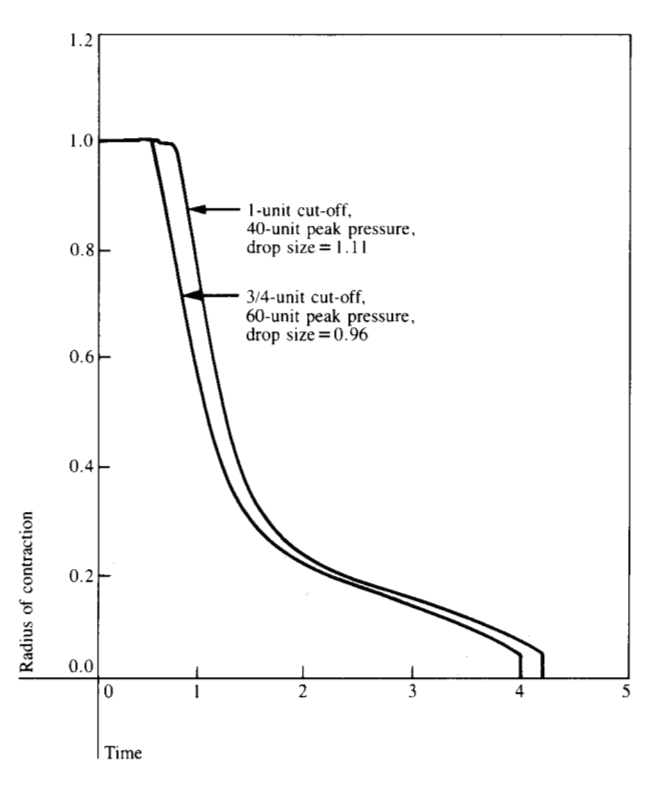


Figure 8 Comparison of contraction radii for two variations of pressure history for R/W = 3 calculations. Sharp break-off is artifically set to occur at a contraction radius of one grid distance.

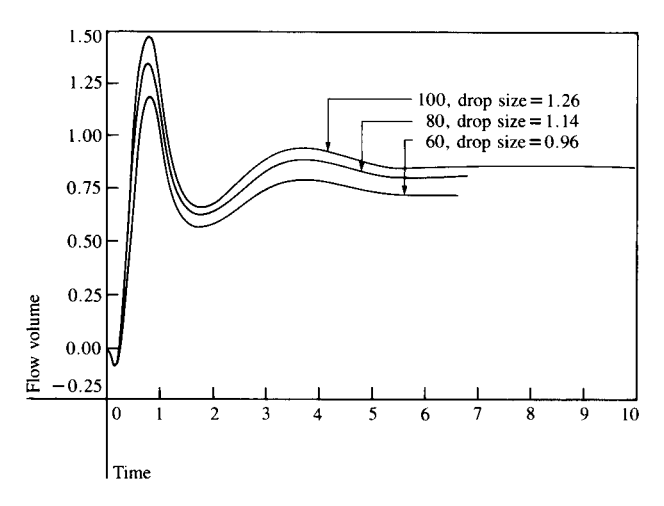


Figure 9 Normalized volume flow at nozzle outlet showing both retracted and forward flow. Normalized drop sizes exceed final flow volume because *computed* final meniscus does not terminate at outlet.

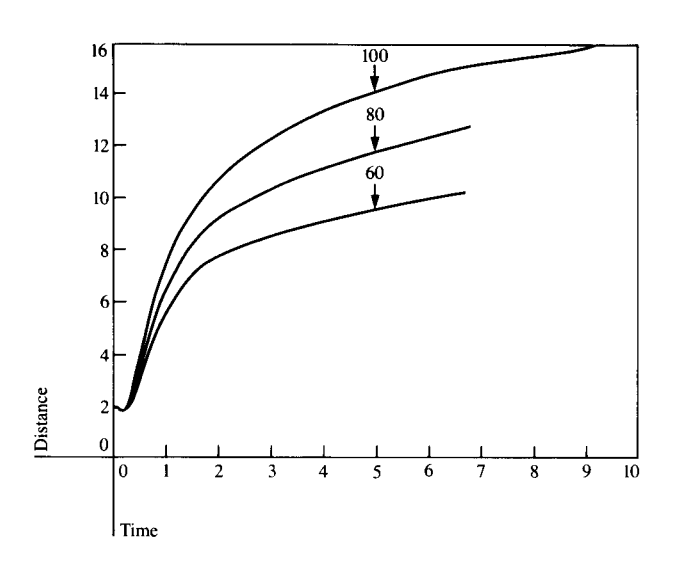


Figure 10 Motion of leading edge for jets with R/W = 3 and given peak pressures.

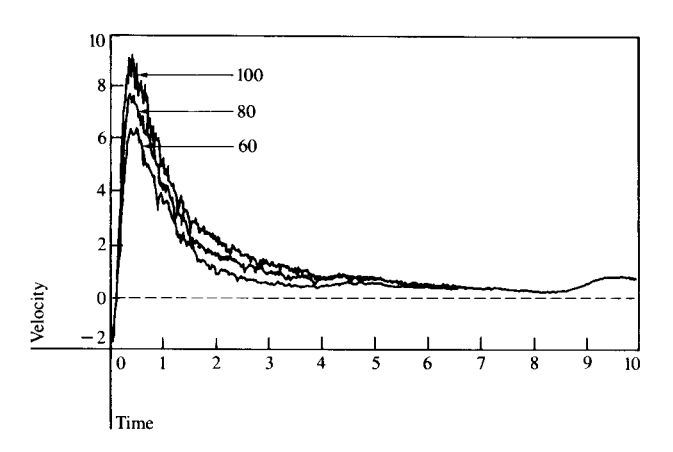


Figure 11 Velocity of leading edge for jets with R/W = 3 and given peak pressures.

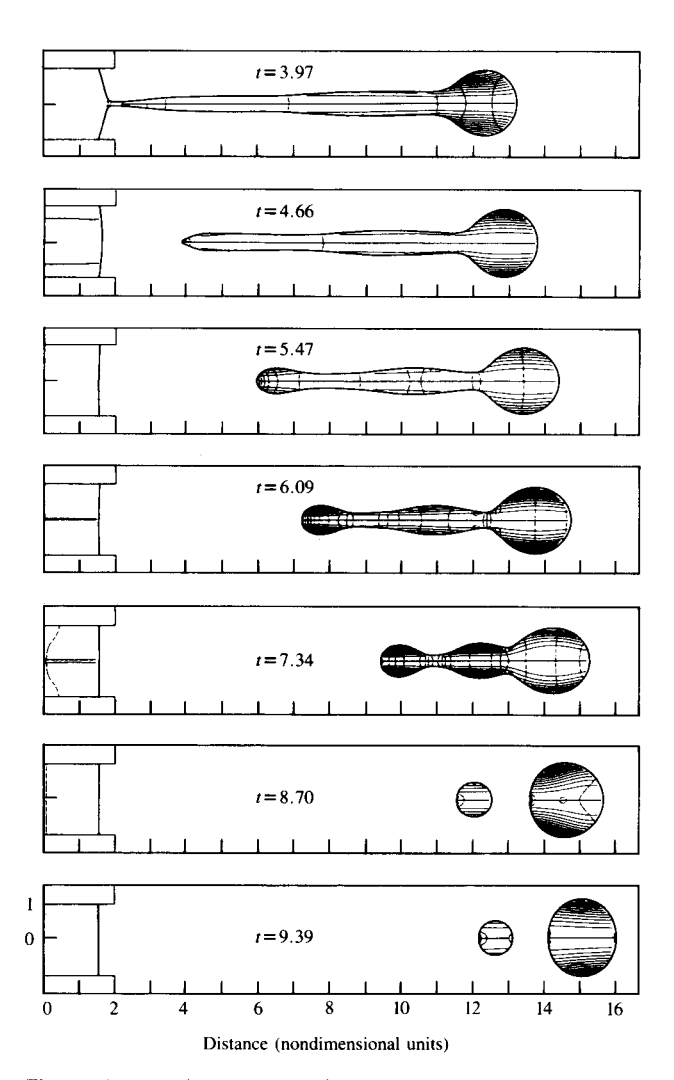


Figure 12 Late time sequence of jet development for R/W = 3 and 100-unit peak pressure. Plot data are given in Table 5.

the net impulse was based upon equal flow volumes. This is in spite of the fact that the peak velocities are quite different. Clearly, if the negative pulse were made equal or greater in magnitude to the positive pulse, a quicker break-off would occur, permitting higher velocities to be achieved in the final drop by benefiting more from those early peak velocities.

There is, of course, more to be discussed concerning the physics of the flows. The behavior of variables other than P and Q is a story in itself. Their behavior is by no means superfluous or of little interest since fundamental aspects of dynamics both at the boundaries and internally are tied up in them, as is the success of the calculation. Vorticity, for example, is not only manifested in the nozzle boundary layer but also emanates from the free surface, giving second order effects there. This is likewise true of normal stresses that have their origin in deformations taking place at the boundaries.

Table 5 Plot parameters for Figure 12.

Time	Plot interval Q	$Q_{\it min}$	Q_{max}	Plot interval P	P_{min}	P_{max}
3.97	1/32	-0.03	0.38	2	-0.73	17.3
4.66	1/32	-0.05	0.34	4	0.00	32.3
5.47	1/32	-0.01	0.26	1	-0.05	10.1
6.09	1/64	0.00	0.22	1/2	-0.14	7.01
7.34	1/64	0.00	0.16	1/2	-0.15	6.84
8.70	1/32	-0.00	0.42	1/2	-0.04	4.54
9.39	1/32	0.00	0.39	1/2	-0.00	4.51

To truly understand their influence, one needs to perform calculations that, say, artificially leave these variables out to provide a contrasting flow behavior. This is a unique capacity of numerical solution and will be an important tool for future growth of our understanding.

Conclusions

It is believed that the numerical programs, as they now stand, are adequate for treating laminar jets as required for ink jet printing. While added features could improve the scope of the calculations, this should be postponed for future consideration as the need dictates. The next step planned is to use actual laboratory pressure histories so that physical data can be obtained, from the calculations, for the experimental hardware at hand. If dependable results are obtained, further steps of refinement in the numerical treatment can follow. The numerical method here described is not a tool for finding an operating window. It is too slow a procedure for that purpose. It can provide insight and understanding that can focus laboratory experiments but it cannot stand alone. This is evident from the idealized pressure histories that are employed here. Clearly, numerical experiments could be carried out with pressures that would fracture laboratory materials, without the results telling us that this is the case. While even such results would have comparison value, we need also to know if they are meaningful in practice. The results given here are meant to suggest properties of the flow that may be useful in development and design problems in the laboratory. We first demonstrated the effect of fluid properties and then the effect of different pressure histories driving the jets. For smaller R/W ratios, one must employ stronger driving pressures. This, however, may be offset in that improved drop integrity appears likely here with the smaller ratio and is so indicated in the laboratory.

Acknowledgment

The author wishes to acknowledge the many discussions, relating the work to laboratory experiments, with Francis C.

Lee and Ross N. Mills. Also, acknowledgment is given to Frank E. Talke and David B. Bogy relating to discussions of theory. Numerous details emerged from these interactions that were crucial to success of the numerical calculations.

References

- F. H. Harlow and J. E. Welch, "The MAC Method: A Computer Technique for Solving Viscous, Incompressible Transient Fluid Flow Problems Involving Free Surfaces," *Phys. Fluids* 8, 2182 (1965).
- G. L. Ream, IBM Information Systems Division, Boulder, CO, private communication.
- F. E. Talke, IBM Research Division, San Jose, CA, private communication.
- J. E. Fromm, "Finite Difference Computation of the Capillary Jet, Free Surface Problem," *Lecture Notes in Physics* 141, pp. 188–193, Seventh International Conference on Numerical Methods in Fluid Dynamics, Springer-Verlag, Berlin, 1981.
- J. E. Fromm, "A Numerical Study of Drop-on-Demand Ink Jets," Proceedings of the Second International Colloquium on Drops and Bubbles, NASA JPL Publication 82-7, California Institute of Technology, Pasadena, 1982.
- J. E. Fromm, "Free Surface Calculation with Application to Drop and Layer Spreading," *Research Report RJ-3871*, IBM Research Laboratory, San Jose, CA, 1983.
- J. E. Fromm, "A Numerical Study of Capillary Spreading of a Liquid Layer," Research Report RJ-3886, IBM Research Laboratory, San Jose, CA, 1983.

Received September 28, 1983; revised November 29, 1983

Jacob E. Fromm IBM Research Division, 5600 Cottle Road, San Jose, California 95193. Mr. Fromm joined the San Jose Research laboratory in 1966. He received his B.S. in physics from the University of Colorado, Boulder, in 1953 and his M.S. in physics from the University of California at Los Angeles in 1955. His research work has been in the area of computational fluid dynamics. This work began while he was at the Los Alamos Scientific Laboratory, where he was on the staff from 1956 to 1966. His early work was on calculations of the Karman vortex trail, which appeared in Scientific American, and Bernard convection; recent work has been on capillary flows.